PHYSICAL REVIEW C VOLUME 24, NUMBER 1 JULY 1981

Inclusive reactions of pions on nuclei

R. D. McKeown, S. J. Sanders, J. P. Schiffer,* H. E. Jackson, M. Paul,† J. R. Specht, and E. J. Stephenson‡
Argonne National Laboratory, Argonne, Illinois 60439

R. P. Redwine
Massachusetts Institute of Technology, Cambridge, Massachusetts 02139

R. E. Segel
Northwestern University, Evanston, Illinois 60201
(Received 15 January 1981)

A systematic set of measurements of pion and proton yields from pion reactions on nuclei $4 \leq A \leq 180$ has been performed for incident pions in the $\Delta(3,3)$ energy region. Detailed energy spectra for protons at many angles were obtained along with inclusive pion yields. The implications of general features of these data for the pion absorption and scattering processes are discussed.

[NUCLEAR REACTIONS ^{4}He, ^{6}Li, ^{9}Be, ^{12}C, ^{27}Al, Ni, ^{181}Ta, $(\pi^\pm, p)$, $(\pi^\pm, \pi^{\pm\prime})$ inclusive; $E_{\pi^\pm}$=100, 160, 220 MeV; $30° \leq \theta \leq 150°$; $d^2\sigma/d\Omega dE_p$, $E_p \geq$ 50 MeV.]

INTRODUCTION

The objective of this experiment was to collect more complete data than currently available on inclusive proton spectra from pions incident on nuclear targets in the Δ resonance region. Such nuclear spectra constitute perhaps the most detailed evidence we can obtain to study the nature of pion absorption in nuclear matter. The distribution of protons in energy and angle and the differences in protons produced by π^+ and π^- interactions are intimately related to the pion interaction mechanism. The principal limitation in our interpretation of these data is our ignorance regarding the transparency of the nuclear medium for nucleon propagation and indeed the conflict between experimental data, which indicate rather long mean free paths of 5—10 fm, and theoretical expectations of around 2 fm.[1] Earlier papers on this line of investigation under more limited experimental condictions have been published[2,3] and the results of the analysis of proton rapidities from the present experiment were also published in the literature.[4] In the present paper we wish to show the overall features of the data and make some simple observations regarding the results. Inclusive data, with no energy information, were also obtained for charged pion scattering and are included here.

EXPERIMENTAL METHOD

The experiment was performed at the low-energy pion channel of the Clinton P. Anderson Meson Physics Facility (LAMPF). The pion beam was typically 2 cm × 2 cm in cross section at the target with a momentum resolution of ~1%. Measurement of the incident pion flux (typically 10^6/sec), was accomplished by counting the absolute yield of ^{11}C activity induced in samples of plastic scintillator exposed to the beam. The uncertainty in the published ^{11}C activation cross sections limits this method to ~15% accuracy.[5] During the experiment, the beam flux was monitored continuously by an ion chamber mounted upstream of the target location.

Pions and protons were detected in two three-element telescopes as shown in Fig. 1: one for forward (30°—90°) angles and one at backward (90°—150°) angles. Each telescope consisted of two thin plastic scintillators (S1 and S2) followed by a NaI(Tl) detector all mounted on a movable frame for angular distribution measurements. The plastic scintillators were 0.64 cm (S1) and 1.91 cm (S2) thick and served to define the solid angle (4×10^{-3} sr), limit the region of view (2.5 cm × 2.5 cm at the target location), and provide energy loss information for particle identification. The NaI detectors were both 12.5 cm in diameter, the forward one was 25 cm long, and the backward one was 12.5 cm long; they gave total energy information for protons which stopped in these counters ($E_p < 300$ MeV at forward angles, $E_p < 210$ MeV at backward angles).

Measurements were performed using six solid targets (^{6}Li, Be, C, Al, Ni, and Ta) and a previously described liquid helium (^{4}He) target.[2] The targets were typically 1 g/cm^2 thick. The narrow field of view of the particle telescopes eliminated background from the target frames (for solid targets) and end windows (for the liquid

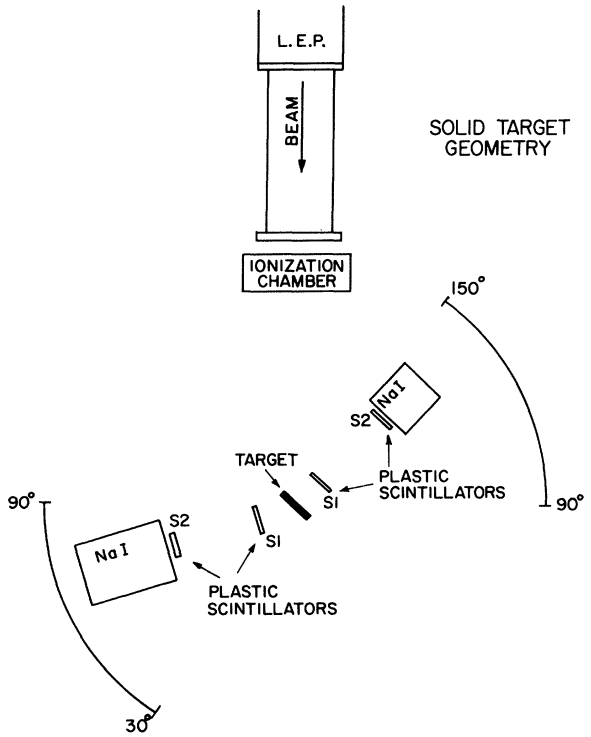

FIG. 1. A schematic of the experimental apparatus. The plastic scintillators defined the solid-angle element seen by the NaI detector.

helium target) at all angles of observation. For the ^{6}Li target, which was contained between sheets of Mylar, a blank Mylar holder was also measured. A typical residual background of ~1—3% was observed for the ^{4}He target during empty cryostat runs.

The event triggers were coincident signals in $S1$ and $S2$ for either telescope during the LAMPF beam pulse. Pulse heights and relative timing information were obtained for all elements of each telescope and processed using an on-line computer. The raw data were also written on magnetic tape for later analysis.

Energy calibration of the detectors was accomplished using protons from the $\pi+p$ elastic scattering process and $\pi^+ + d \rightarrow 2p$ reaction. This energy calibration was accurate to ~5%. The gain stability of all detector elements was monitored using a light-emitting diode (LED) pulsing system which also facilitated a measurement of the dead time of the system.

DATA ANALYSIS

A three-dimensional display of a spectrum is shown in Fig. 2. The events were binned into two-dimensional arrays of two different types

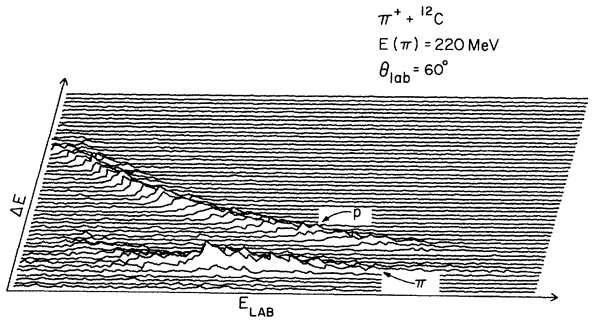

FIG. 2. Three-dimensional display of the $^{12}C + \pi^+$ data at 60°, $T_\pi = 220$ MeV. The ridges of protons and pions are clearly evident; the pions are not stopped in the NaI detector.

for each telescope. The two types were for "low-range" events (stopped in $S2$) and "high-range" events (more than 5 MeV deposited in NaI). The arrays were ΔE vs E spectra; protons and pions (the only major particle groups observed) could be identified by their different respective energy losses in the $S1$ and/or $S2$ counters (see Fig. 2). Pion yields were extracted directly from the spectra of $\Delta E(S2)$ vs E(NaI).

For protons the arrays were corrected for nuclear reaction losses in the counters. Each ΔE "row" was corrected separately by shifting a fraction of the yield from below a given pulse height into the channel corresponding to that pulse height. This contribution was varied linearly with the channel number in order to approximate the NaI response given in Ref. 6. The low-range protons were simply summed and assigned an aver-

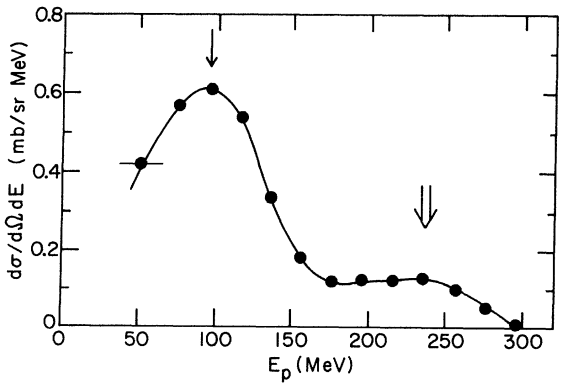

FIG. 3. A typical proton spectrum from $^{12}C(\pi^+, p)$ at 30°, $T_\pi = 220$ MeV. The horizontal bar on the first point indicates the larger bin for these data, the other points are equally spaced. The single arrow shows the energy for proton recoils from $\pi+N$ scattering, the double arrow for protons from $\pi + 2N \rightarrow 2N$ absorption.

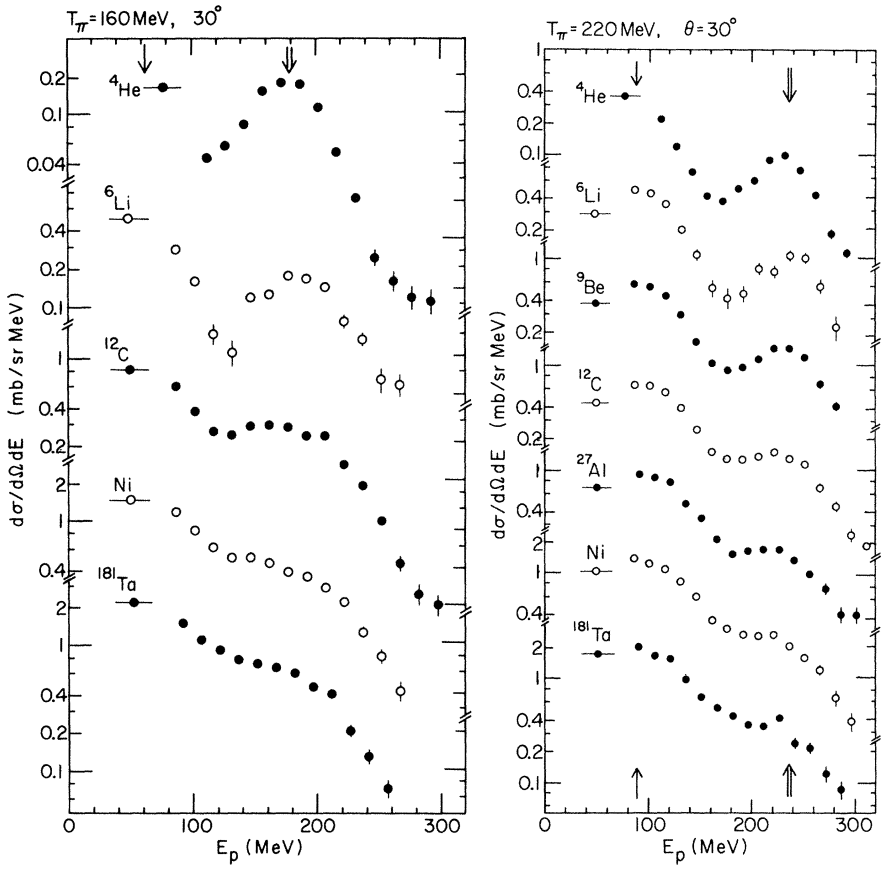

FIG. 4. Proton spectra from all targets for $\theta = 30°$, $T_{\pi^+} = 160$, 220 MeV. The horizontal bar on the lowest energy points indicates the larger bin for these data, the other points are equally spaced. Error bars, where shown, indicate statistical errors only. The single and double arrows indicate proton energies expected from $\pi + N$ scattering and $\pi + 2N \rightarrow 2N$, respectively.

age energy because of poor total energy information in $S2$ for these events. The high-range protons were projected out as an energy spectrum with the low-range proton yield appended to the low low-energy and of the spectrum as a single point. This spectrum was then corrected for average energy loss in the target and normalized the pion flux, solid-angle, target thickness, and dead-time information to yield proton energy spectra, an example of which is shown in Fig. 3. For $T_p > 100$ MeV the resolution is $\Delta T/T < 10\%$ and is determined by the NaI detector. Below $T_p \sim 100$ MeV the resolution is degraded by the effects of the finite target thickness to about 10 MeV.

PRESENTATION OF THE PROTON DATA

The energies and targets for which data were obtained in the present experiment are shown in Table I, generally for the angles of 30°, 45°, 60°, 90°, 120°, and 150°. For ^{4}He, data at additional angles were also obtained.

The underlying reaction mechanisms show up most clearly when the protons are emitted in the forward direction, e.g., at 30°, as in Figs. 4 and 5. For π^+ on ^{4}He there is a well defined maximum at the proton energy (~235 MeV for T_π = 220 MeV) corresponding to the $(\pi, 2N)$ absorption mechanism, but this peak rapidly degenerates into a shoulder in heavy nuclei. Another peak appears at ~95 MeV near the energy expected

TABLE I. Data obtained with π^+ and π^- beams.

Target	T_π (MeV)	100	160	220
^{4}He		×	×	×
^{6}Li		×	×	×
^{9}Be		×		×
^{12}C		×	×	×
^{27}Al		×		×
^{nat}Ni		×	×	×
^{181}Ta		×	×	×

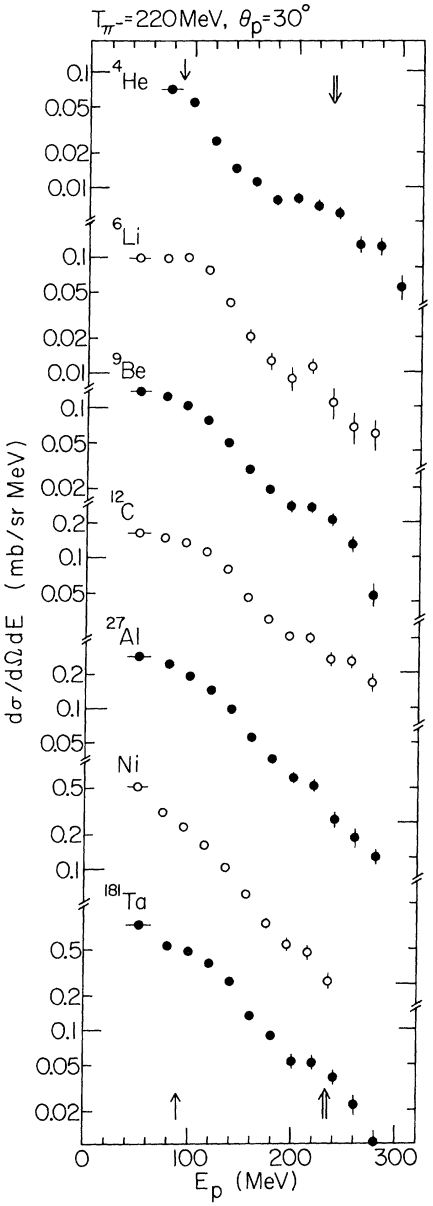

FIG. 5. Proton spectra from all targets for $\theta = 30°$, $T_{\pi^-} = 220$ MeV. See Fig. 4 for notation.

from quasifree π-N scattering. The dependence of the proton yield on the target atomic weight is plotted for the higher proton energy region of the 30° spectra for $T_\pi = 220$ MeV in Fig. 6. No attempt has been made to fit model-dependent peak shapes to the spectra—what is plotted is simply the proton cross section for $T_p > 160$ MeV. What is qualitatively noted in Fig. 4 is explicitly clear here—the high-energy yield changes much more slowly with A than the bulk of the proton yield. The data for π^- are presented in Fig. 5 and they show the two-nucleon absorption peak to

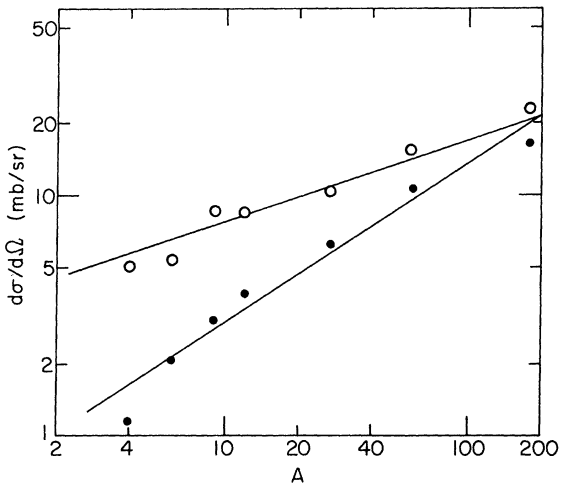

FIG. 6. The A dependence of high-energy ($T_p > 160$ MeV) protons from π^+ at 30° is shown as open circles. The solid points represent the total angle-integrated proton yield for $T_p \gtrsim 40$ MeV divided by 100; both curves are for $T_{\pi^+} = 220$ MeV.

a much lesser extent.

Since we observe a well-defined peak corresponding to quasideuteron absorption in the forward angle proton spectra from ^{4}He, we have further analyzed the behavior of these protons. The proton yield in this peak was extracted from the data by simply setting a lower energy cut at the minimum below the peak and summing the spectrum above this energy. We estimated the uncertainty in this procedure by taking a smoothly falling background under the peak and assigning an uncertainty to the peak yield of ±50% of the extrapolated background. No subtraction was made. The results are shown in Fig. 7 as a function of

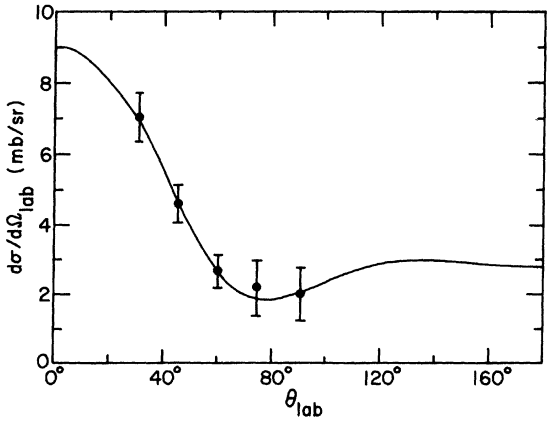

FIG. 7. The angular distribution of protons in the quasideuteron absorption peak for ^{4}He at $T_{\pi^+} = 220$ MeV. The solid line is the angular distribution of protons from $\pi^+ + d \rightarrow 2p$ at $T_\pi = 220$ MeV multiplied by 3.8.

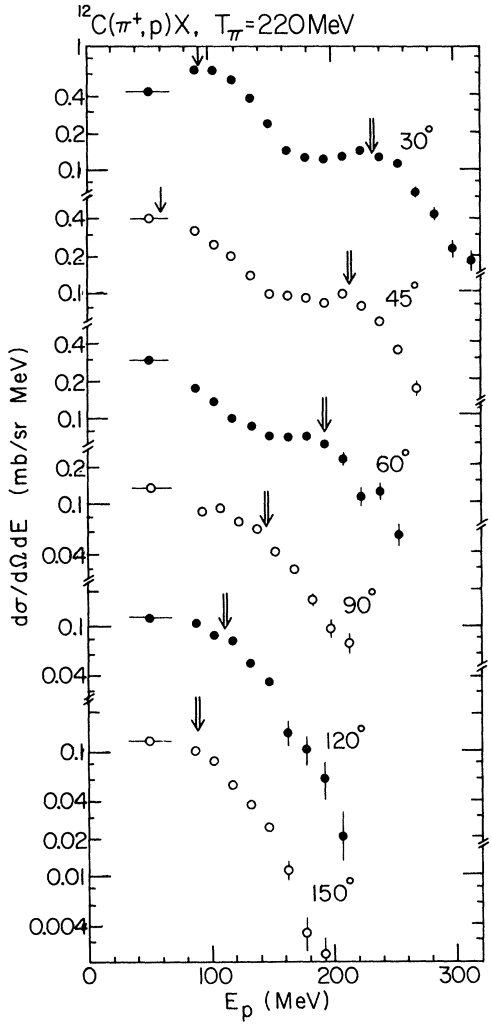

FIG. 8. Proton spectra from $^{12}C + \pi^+$ as a function of angle. Notation is the same as in Fig. 4.

angle, along with the scaled (×3.8) deuteron cross section[7] which is shown as a solid line. The proton yield in this peak clearly shows the same angular distribution as the $\pi^+ + d \to 2p$ process. The scaling factors are 3.8 ± 0.5 at $T_\pi = 220$ MeV, 3.0 ± 0.5 at 160 MeV, and 3.1 ± 0.5 at 100 MeV. These values agree very well with $3\frac{3}{8}$ calculated in the Appendix, assuming no dependence on the spin coupling of the initial nucleon pair and no radial wave function (nuclear density) dependence to the $(\pi, 2N)$ cross section. If we scale the deuteron absorption cross section by these factors, we obtain the quasideuteron absorption cross section for ^{4}He. The results are 21 ± 4, 35 ± 6, and 30 ± 5 mb at $T_\pi = 220$, 160, and 100 MeV, respectively. Previous measurements of the ^{4}He pion absorption cross sections give $\sigma_{abs} \sim 60$—80 mb in

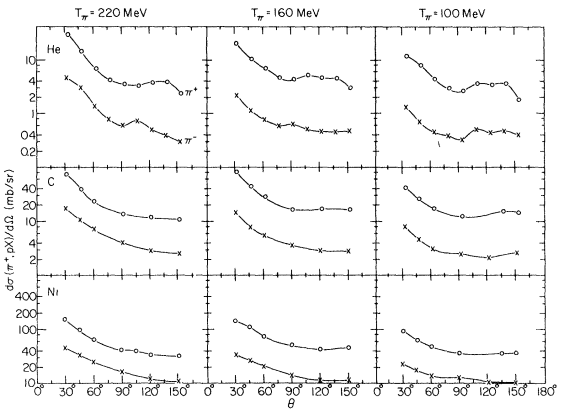

FIG. 9. Angular distribution for the observed proton yields for ^{4}He ($T_p \gtrsim 70$ MeV), ^{12}C, and Ni ($T_p \gtrsim 40$ MeV). The lines connect the points.

this energy region.[8] This implies that only about $\frac{1}{2}$ the absorption cross section results in an unperturbed quasideuteron mechanism.

The peak in ^{4}He is broadened by the Fermi motion of the nucleons; the width of the peak is well reproduced by a Fermi distribution with $p_F \cong 100$ MeV/c. The angle dependence of the proton data is shown for one case, ^{12}C with $T_{\pi^+} = 220$ MeV, in Fig. 8, The πN quasifree scattering should contribute little for $\theta > 60°$ and the proton yield should predominantly originate from absorption only.

Examples of angular distributions are shown in Fig. 9. An attempt was made to obtain the total proton yield by fitting a smooth curve to these distributions and integrating them, but with no attempt to extrapolate the yield to proton energies in the unobserved region below the experimental cutoff. The total proton cross sections are listed in Table II and the A dependence for 220 MeV is shown in Fig. 6. A dependences for the various data are given in Table III. Because of the isospin dependence of the π-N interaction the ratio of protons yields from π^+ and π^- is of particular interest. In Fig. 10 we show the π^+/π^-

TABLE II. Angle-integrated proton yields in mb. $T_p \gtrsim 70$ MeV for He and ≥40 MeV for all other targets.

Target	T_{π^+}=100	160	220	T_{π^-}=100	160	220
^{4}He	57	92	98	7.4	10.5	16.9
^{6}Li	103	189	166	14	31	39
^{9}Be	170		250	25		53
^{12}C	240	370	310	44	71	80
^{27}Al	380		480	90		140
Ni	610	860	790	161	220	265
^{181}Ta	890	1280	1220	260	340	420

TABLE III. A^n dependence of various yields.

T_π (MeV)	Angular range	Proton energy range	A^n dependence[a] π^+	π^-
100	Angle integrated	All observed	0.69(0.61)	0.93(0.85)
160	Angle integrated	All observed	0.65(0.55)	0.85(0.69)
220	Angle integrated	All observed	0.64(0.58)	0.80(0.71)
160	30°	T_p>140 MeV	0.38(0.34)	0.54(0.47)
220	30°	T_p>200 MeV	0.38(0.37)	0.51(0.48)
160	30°	T_p<140 MeV	0.65(0.46)	0.54(0.47)
220	30°	T_p<200 MeV	0.55(0.50)	0.67(0.57)
100	Angle integrated for backward hemisphere	Pions	0.44(0.49)	0.47(0.54)
160			0.42(0.47)	0.47(0.52)
220			0.50(0.52)	0.50(0.53)

[a] Parentheses represent n values where ^{4}He was not included.

ratio for ^{4}He, ^{12}C, and Ni at three pion energies at which data were obtained. In addition the A dependence of the total proton yield ratios (π^+/π^-) is plotted in Fig. 11, but as a function of the nuclear radius (assumed to be $1.2A^{1/3}$).

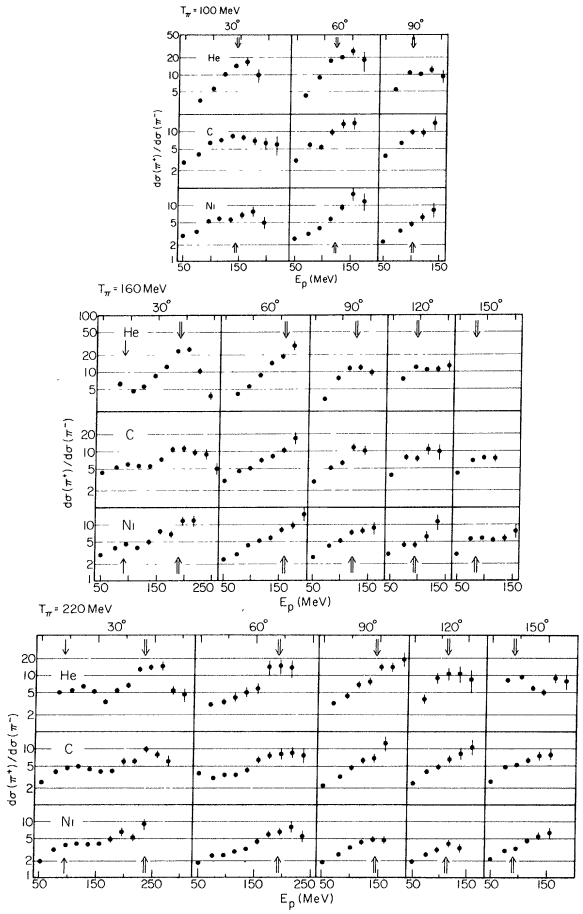

FIG. 10. Ratio of proton yields seen with π^+ to those with π^-. Statistical errors are shown. The meaning of the errors is in Fig. 4.

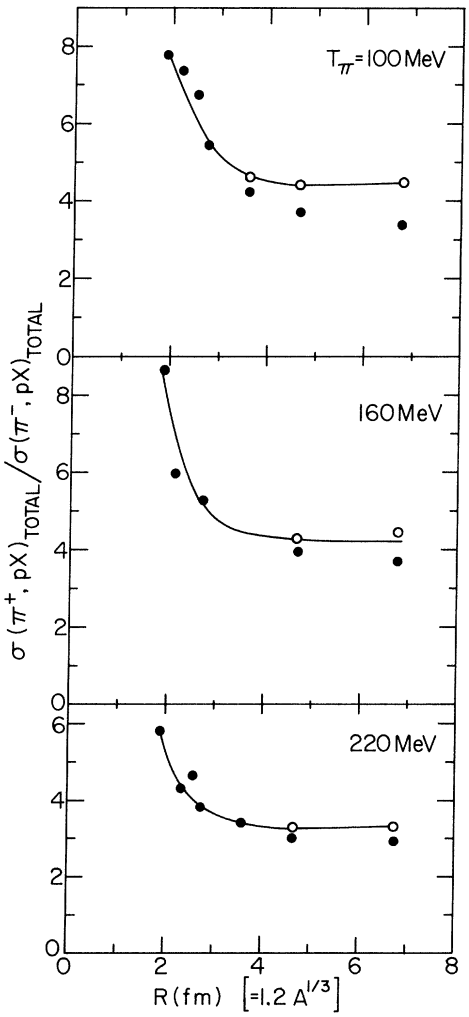

FIG. 11. Ratio of angle integrated total proton yields seen with π^+ to those with π^-, as a function of nuclear radius. The open circles include the Coulomb correction $(T_\pi+V_c)/(T_\pi-V_c)$, where $V_c=Ze^2/R$. The line is to guide the eye.

DISCUSSION OF THE PROTON DATA

For the conventional two-nucleon absorption model proceeding through the (3,3) resonance, one expects the ratio of the number of energetic protons with π^+ to those with π^- for a heavy nucleus to be, for uncorrelated nucleons,

$$R_{2N}=\frac{10Z(A-Z)+(A-Z)(A-Z-1)}{Z(Z-1)}.$$

For ^{4}He the isospin correlations are important; one obtains $R_{2N}(^4\mathrm{He})=27$ as shown in the Appendix.

The value for R_{2N} is given in Table IV for our targets. It is 27 for ^{4}He and would approach 11 asymptotically for a heavy $N=Z$ target, but, in fact, never reaches this value because of the neutron excess.

Similarly for the quasifree process, using the Clebsch-Gordan coefficients for the 3,3 resonance, we have

$$R_{\pi N}=\frac{9Z+2(A-Z)}{Z},$$

which is between 11 and 12 for all our targets. The expression above would be modified slightly if the measured π-N cross section were used instead, for $T_\pi=220$ MeV and $\theta_{\mathrm{lab}}=30°$ one would get $[7.8Z+1.79(A-Z)/(1.01Z)$, which is about 15% lower than the above expression for $R_{\pi N}$.

In Fig. 10, the experimental π^+/π^- ratios, at the proton energy corresponding to two nucleon absorption at forward angles, are consistently 70—90% of the calculated R_{2N} values listed in Table IV. However, at backward angles the experimental ratios are typically only about 50% of R_{2N} and show no clear enhancement at the $(\pi, 2N)$ energies. The backward angle energetic protons must originate from pion absorption events, and the low experimental π^+/π^- ratios indicate that the pure unperturbed $\pi+2N\rightarrow 2N$ process is not dominant (even in ^{4}He).

Assuming that pion absorption proceeds through Δ formation, we are led to the conclusion that the final state often consists of several nucleons (rather than just two). This will lower the π^+/π^- ratios and yield energy spectra with more nucleons at lower energies than the pure quasideuteron process. This conclusion is also consistent with the rapidity analysis of these data in Ref. 4. The nucleons from quasifree π-N scattering are not cleanly observed in inclusive measurements. The fact that the π^+/π^- ratios at forward angles in the quasifree π-N energy region are far below the $R_{\pi N}$ values of Table IV supports this conclusion (see Fig. 10). A more detailed interpretation of these proton spectra requires assumptions about Δ propagation and decay in the nuclear medium and rescattering of the final-state nucleons.

TABLE IV. Predicted ratios for two-nucleon absorption (R_{2N}) and quasifree scattering ($R_{\pi N}$).

Target	R_{2N}	$R_{\pi N}$
^{4}He	27	11.0
^{6}Li	16	11.0
^{9}Be	18.3	11.5
^{12}C	13.0	11.0
^{27}Al	12.8	11.2
Ni	12.6	11.2
^{181}Ta	17.2	12.0

PRESENTATION OF THE PION DATA

The inclusive pion scattering yields, for both incident π^+ and π^- beams, were obtained at each angle and energy for the solid targets. Although energy spectra for the scattered pions were not obtainable, the pions above an energy threshold $E_\pi\sim 20$ MeV were cleanly resolved in the $\Delta E(S2)$ vs E(NaI) spectra, as shown in Fig. 2, and could be summed for the inclusive yields. As an example, the angular distribution for $^{12}\mathrm{C}(\pi^+,\pi^{\pm})$ scattering at $E_{\mathrm{lab}}=160$ MeV is plotted in Fig. 12, with the average of the free π^+p and π^-p cross sections plotted alongside scaled to the data. Since these inclusive pion yields include the effects of elastic

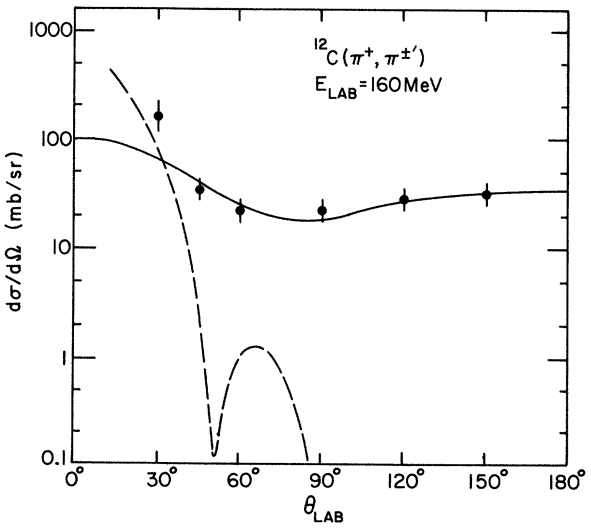

FIG. 12. Angular distribution of charged pions scattered by ^{12}C with T_π=160 MeV. The dashed line represents elastic scattering from ^{12}C (Ref. 9), the solid curve is the average of $\pi^+ + p$ and $\pi^- + p$ scattering, normalized to the data. The errors include estimates of all uncertainties.

TABLE V. Inclusive charged pion inelastic scattering yields in mb integrated over the backward hemisphere. The uncertainties in the absolute cross sections are estimated at ±15%, the *relative* uncertainties for a given pion beam energy and charge (among the solid targets) are ≤5%; the ^{4}He data depend on an independent calibration and their uncertainty relative to all others are always ±15%.

	T_π (MeV)	100^+	100^-	160^+	160^-	220^+	220^-
^{4}He		45	39	73	64	59	59
^{6}Li		77	68	132	109	85	87
^{9}Be		100	113			108	136
^{12}C		123	104	170	143	131	131
^{27}Al		154	144			176	178
^{nat}Ni		242	220	317	287	280	272
Ta		355	454	547	599	459	561

scattering, we have indicated by the dashed curve the measured elastic scattering angular distribution at $E_{lab} = 163$ MeV obtained using the Energetic Pion Channel and Spectrometer (EPICS)[9]; clearly the elastic scattering yield is negligible past $\theta_{lab} > 45°$.

Total inclusive charged pion yields were obtained for the backward hemisphere by integrating the data for $\theta \geq 90°$. One may alternatively normalize the data at back angles to the shape of the average of the (π^+-p) and (π^--p) angular distribution and estimate the total inelastic yield; this procedure yields total inelastic charged pion yields ~1.89, 2.39, and 3.32 times the values in Table V for

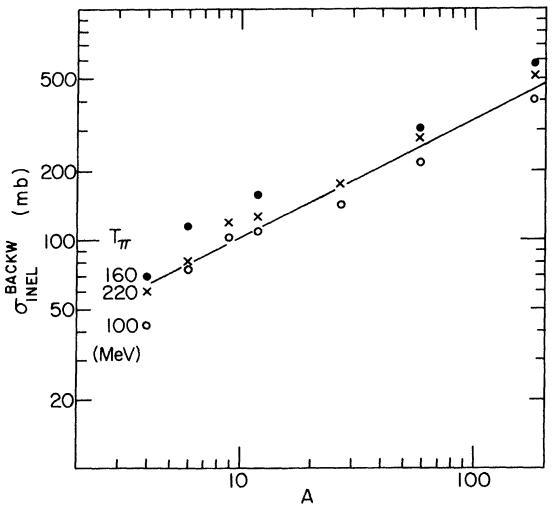

FIG. 13. The A dependence of the inelastic charged pion scattering integrated over the backward hemisphere $\theta_{lab} \geq 90°$. The points shown are the average values for π^+ and π^-.

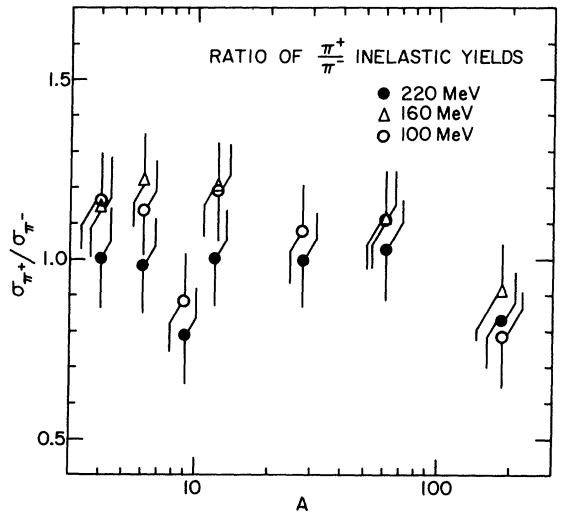

FIG. 14. Ratios of the inelastic charged pion yields in the backward hemisphere, π^+ to π^-, with systematic errors shown.

$T_\pi = 100$, 160, and 220 MeV. However, the assumption that the inelastic yield follows the free π-nucleon scattering is likely to be a strong oversimplification. The measured backward inelastic scattering yield is in reasonable agreement with the published values of Refs. 10 and 11.

The total cross sections for the backward hemisphere are plotted in Fig. 13. The slopes of the A dependences are included in Table III. Finally, the π^+/π^- ratios for the backward-hemisphere yields are plotted in Fig. 14, where the error bars from the absolute cross section measurements are seen to be overwhelming because of the near equality of the cross sections. This ratio was renormalized, requiring it to be equal to one for ^{12}C, and is shown in Fig. 15, thus making systematic trends more clearly visible.

DISCUSSION OF THE PION DATA

The average A dependence of the π^+ and π^- data is ~$A^{0.51\pm0.03}$, slower than geometrical ($A^{0.67}$) and consistent with the fact that absorption increases faster than $A^{0.67}$.[11] Absorption is apparently taking a larger and larger share of the reaction cross section with increasing target size, at the expense of inelastic scattering.

For the π^+/π^- ratios the Coulomb effect needs to be considered,[12] which may be approximated by a simple classical expression. For a repulsive Coulomb field $\sigma \sim (1 - V_c/T_\pi)$, where T_π is the pion kinetic energy and $V_c = Ze^2/R$ is the Coulomb field at the radius R where the pion starts to interact. For an attractive Coulomb field $\sigma \sim (1 + V_c/T_\pi)$. The π^+/π^- ratios should therefore be corrected for Coulomb effects by $(T_\pi + V_c)/$

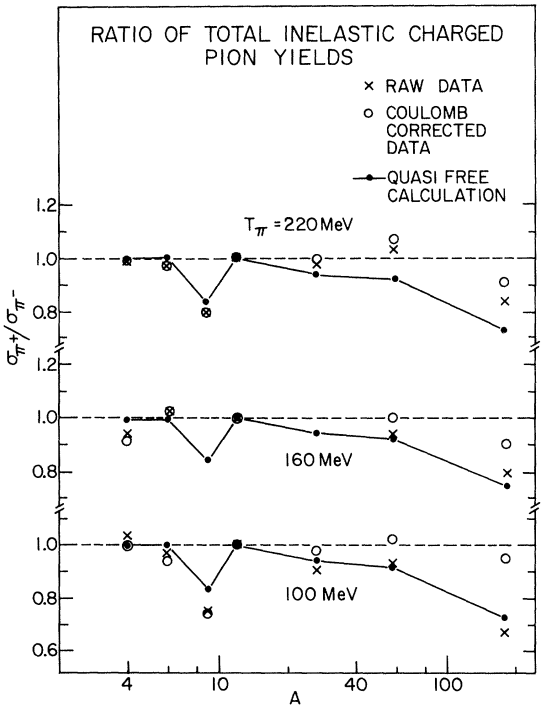

FIG. 15. Ratios of the inelastic charged pion yields in the backward hemisphere, π^+ to π^-. The ratios for each energy are normalized by requiring ^{12}C to have a ratio equal to one. The open circles have the Coulomb correction $(T_\pi + V_c)/(T_\pi - V_c)$ applied, and the small dots with the connecting lines represent $(9Z+N)/(9N+Z)$.

$(T_\pi - V_c)$, as was done in Fig. 14.

One may also expect the neutron excess to show up because of Δ dominance. This would cause the cross section to behave as $(9Z+N)/(9N+Z)$. Such an effect is evident only for the relatively large neutron excess of ^9Be. For ^{181}Ta, our other target with an appreciable neutron excess, there seems to be only a small enhancement of π^- scattering after Coulomb effects are removed. It seems reasonable to argue that here the nucleus is black in any case and the amount of π^+ vs π^- inelastic scattering is determined by the competition between absorption and the inelastic process. If it were not for absorption the π^+ and π^- inelastic cross sections would both be geometrical and thus equal.

CONCLUSIONS

This systematic study of inclusive charged-particle yields from pion-induced reactions indicates that the reaction of pions with nuclei is quite complex. In particular, the pion absorption process seems to lead to very complicated final states of energetic nucleons which are difficult to characterize in terms of simple models. In addition, the absorption process strongly affects the inelastic pion yields and, in fact, dominates the reaction cross section in heavy nuclei. Nevertheless, some simple analyses of these data do illuminate some of the qualitative aspects of the interaction of pions with nuclei.

For very light nuclei (^4He), the quasideuteron absorption mode is quite evident in the final state protons. The kinematics, angular distribution, and π^+/π^- ratios of these protons are in very good agreement with expectations. However, even in ^4He the total yield of these protons is small compared to the absorption cross section. The lower energy protons are not understood (forward and backward angles), but certainly are not attributable to only pure quasifree π-N scattering. Some of them are undoubtedly due to π absorption.

In heavier nuclei, the two-nucleon peak becomes a small fraction of the proton yield (a few percent in Ta). The kinematics and π^+/π^- ratios of the general proton spectrum indicate that perhaps a multinucleon final state is the result of the absorption process. Because of this, the A dependence of the proton yields themselves is difficult to interpret.

The pion yields generally appear to follow the free π-N angular distribution at backward angles. However, the forward-angle protons from quasifree π-N scattering do not appear unambiguously in the proton spectra. Coincidence measurements in the quasifree region are clearly needed to investigate this process. The A dependence of the pion yields are typically $A^{\sim 0.5}$, consistent with increasing dominance of the reaction cross section by absorption. The ratios of π^+/π^- pion yields show some general Coulomb and isospin effects, as expected.

The detailed analysis of the proton spectrum is hindered by our lack of knowledge about nucleon propagation in nuclear matter at these energies. Consistent analyses of $(e,e'p)$, (γ,p), (p,p'), and $(p,2p)$ might give enough information to further interpret the proton spectra obtained in this work.

Tabulations of the differential cross sections reported here are deposited in the Physics Auxiliary Publication Service.[13]

ACKNOWLEDGMENTS

The authors would like to acknowledge the support of the LAMPF operating staff and the technical assistance of J. Worthington. The help of J. Groner and G. Pulawski in reduction of data is gratefully acknowledged. We benefitted from useful discussions with many colleagues, notably D. Kurath and T.S.H. Lee. This work was per-

formed under the auspices of the U.S. Department of Energy and the National Science Foundation.

APPENDIX

We denote the amplitude for $\pi + 2N \to 2N$ by $M(I_a, I_b)$, where I_a (I_b) is the isospin of the initial (final) $2N$ system. Assuming (3,3) dominance and that the amplitudes are independent of the spin coupling of the initial nucleons, we need only consider $I_b = 1$, and there are two amplitudes [$M(0,1)$ and $M(1,1)$] related by

$$M(0,1) = \sqrt{2} M(1,1) . \tag{A1}$$

For a single pair of nucleons, the cross section may be written

$$\sigma(m_\pi, m_1, m_2) = \sum_{I_a} \langle 1 m_\pi I_a i_a | I_b i_b \rangle^2 \times M^2(I_a, I_b) P(I_a) , \tag{A2}$$

in which m_π, m_1, and m_2 represent the pion and initial nucleon charge states ($i_a = m_1 + m_2$) and $P(I_a)$ is the probability of the initial $2N$ system having isospin I_a. The deuteron has $I = 0$, and we obtain a cross section for $\pi^+ + d \to 2p$ of $\sigma(d) = M(0,1)^2$.

In a heavy nucleus, we assume $P(1) = P(0) = \frac{1}{2}$ for the np pairs, and evaluate the expression for the ratio of *proton* yields

$$R_{2N} = \frac{2 \cdot \sigma(1, \frac{1}{2}, -\frac{1}{2}) \cdot N \cdot Z + \sigma(1, -\frac{1}{2}, -\frac{1}{2}) \cdot N(N-1)/2}{\sigma(-1, \frac{1}{2}, \frac{1}{2}) \cdot Z(Z-1)/2} \tag{A3}$$

to obtain the result given in the text. Using the simple ^{4}He wave function with all four nucleons in relative s states, there are four np pairs (three $I = 0$ and one $I = 1$) plus a pp pair and an nn pair. Thus for ^{4}He we evaluate expression (A3) with $P(0) = \frac{3}{4}$ and $P(1) = \frac{1}{4}$ for the np pair term. The result is

$$R_{2N}(^4\mathrm{He}) = \frac{6M(0,1)^2 + M(1,1)^2 + \frac{1}{2}M(1,1)^2}{\frac{1}{2}M(1,1)^2} = 27 . \tag{A4}$$

Similarly, we can calculate the proton yield from $\pi^+ + {}^4$He compared to the deuteron:

$$\frac{\sigma(^4\mathrm{He})}{\sigma(d)} = 3\tfrac{3}{8} . \tag{A5}$$

If, on the other hand, one were to assume a different dependence of the amplitude on the initial coupling of nuclear spins, these ratios would, of course, be different.

---

*Also at the University of Chicago, Chicago, Illinois 60637.

†Present address: Racah Institute, Hebrew University, Jerusalem, Israel.

‡Present address: Indiana University Cyclotron Facility, Indiana University, Bloomington, Indiana 47401.

[1]J. P. Schiffer, Nucl. Phys. A335, 339 (1979).

[2]H. E. Jackson, S. L. Tabor, K.-E. Rehm, J. P. Schiffer, R. E. Segel, L. L. Rutledge, Jr., and M. A. Yates, Phys. Rev. Lett. 39, 1601 (1977).

[3]H. E. Jackson, S. B. Kaufman, L. Meyer-Schutzmeister, J. P. Schiffer, S. L. Tabor, S. E. Vigdor, J. N. Worthington, L. L. Rutledge, Jr., R. E. Segel, R. L. Burman, P. A. M. Gram, R. P. Redwine, and M. A. Yates, Phys. Rev. C 16, 730 (1977).

[4]R. D. McKeown, S. J. Sanders, J. P. Schiffer, H. E. Jackson, M. Paul, J. R. Specht, E. J. Stephenson, R. P. Redwine, and R. E. Segel, Phys. Rev. Lett. 44, 1033 (1980).

[5]B. J. Dropesky, G. W. Butler, C. J. Orth, R. A. Williams, G. Friedlander, M. A. Yates, and S. B. Kaufman, Phys. Rev. Lett. 34, 821 (1975).

[6]D. F. Measday and C. Richard-Serre, CERN Report No. 69-17 (1969).

[7]C. Richard-Serre *et al.*, Nucl. Phys. B20, 413 (1970).

[8]M. Hirata, F. Lenz, and K. Yazaki, Ann. Phys. (N.Y.) 108, 116 (1977).

[9]H. A. Thiessen, Los Alamos Scientific Laboratory Progress Report No. MP-10 (1978).

[10]I. Navon, D. Ashery, G. Azeulos, H. J. Pfeiffer, H. K. Walter, and F. W. Schlepütz, Phys. Rev. Lett. 42, 1465 (1979).

[11]D. Ashery, I. Navon, G. Azeulos, H. K. Walter, H. J. Pfeiffer, and F. W. Schleputz, Phys. Rev. C 23, 2173 (1981).

[12]For proton spectra such corrections were not made, because the experimental ratios varied much more drastically. For the inelastic pion ratios, the Coulomb correction *is* important.

[13]See AIP document No. PAPS PRVCA-24-211-48 for 48 pages of tabulations of the differential cross sections reported here. Order by PAPS number and journal reference from American Institute of Physics, Physics Auxiliary Publication Service, 335 East 45th Street, New York, New York, 10017.